

# An Interpolating H-adaptive Element Free Galerkin Method for Elasticity Problems

Min Wang, Gang Peng, and Xiaohua Zhang\*

**Abstract**—An adaptive element free Galerkin (EFG) method is extended to the analysis of linear elasticity problems. The error estimation of this adaptive analysis is based on the element residual error. The residual-based posterior error estimation of the finite element method (FEM) is directly implemented in the adaptive EFG method, benefiting from the use of the arbitrary polygonal influence domain technique in EFG method. Four benchmark problems of elasticity are tested by this proposed method. The numerical results are close to the exact solutions, and the error estimates are consistent with those in the finite element method.

**Index Terms**—element free Galerkin method, adaptive methods, a posteriori error estimator, element residual error, linear elastic problem.

## I. INTRODUCTION

THE finite element method is a widely used and extensively studied numerical method with simple and compact expressions for nodes and elements. However, those nodes and elements in the solution region must satisfy topological validity and geometric efficiency. It limits its application in some fields such as stress concentration, crack propagation and large deformation, which solutions change sharply in some subdomains.

The meshless method constructs a trial function based on nodal approximation without dividing elements. It has become a crucial numerical tool after the finite element method [1]–[6]. The number and position of nodes are relatively free in the meshless method, the shape function has high-order continuity and flexible form. These characteristics make the meshless method suitable for problems that FEM is not good at, such as the adaptive calculation in high gradient, large deformation and singularity.

The meshless methods are usually classified into two types [4], depending on how the differential equations are approximated. The Galerkin meshless method is developed from the weak form of the governing equations. On the other hand, the collocation method (or particle method) is built using the strong form of the governing equations. Belytschko et al. [1] analyzed the fracture and crack growth problems by element-free Galerkin methods, which led to the rapid development of the meshless method [7]–[9]. This paper mainly focuses on the element-free Galerkin method. In

particular, the moving least square (MLS) method is used to generate the shape function. [10].

The adaptive analysis is an integral part of modern numerical simulations, especially for problems that the solution varies greatly in certain subdomains, such as stress concentration, crack propagation, large deformation, etc. The adaptive analysis aims to obtain better accuracy with a fewer node or to capture the local properties of the discussed problem. It is different from the traditional numerical methods [11], [12]. The meshless method allows for relatively unrestricted configuration, addition, and deletion of field nodes, which makes it easier to do adaptive analysis.

There are usually three types of adaptive analysis algorithms. The first kind is the h-type analysis, which increases the precision of the solution by reducing the size of the elements and increasing the number of nodes. The second kind is the p-type analysis, which increases precision through using higher-order polynomial shape function. In contrast, the third kind, the r-type technique yields a more accurate result by altering the location of the nodes. Although a combination of these can be utilized, the h-adaptive method is the most common approach.

As a widely used numerical algorithm, the adaptive finite element method has also been studied relatively early and maturely. These adaptive analysis types and their various hybrid forms were proposed initially and developed from the finite element method [13]–[15]. A reliable error estimation model is the first crucial issue to be considered in the adaptive analysis [13]–[20]. Residual-based error estimation and recovery-based error estimation are the two main types of a posteriori error estimation. In residual-based techniques, the integration element's residual function is used to estimate the error. While the error estimate in recovery-based methods depends on the solution and its gradient.

The recovery error estimation, however, is the most used error estimation in the adaptive element free Galerkin approach. Recovery-based adaptive researches are widely conducted in EFG [21]–[26]. Chung and Belytschko [21] proposed the recovery error estimation by combining the local and global error, Lee and Zhou [22] introduced a stress-recovery posteriori error estimation, He et al. [24] established the error estimation by the node stresses, Metsis et al. [27] proposed a hierarchical method by introducing the recovered stress [21] into the Z-Z error estimator [14], Kumar et al. [28] proposed a recovery-based method by the natural neighbor Galerkin mesh, Hajjout et al. [26] presented an h-type adaptive method by the Z-Z error estimator, Jannesari and Tatari [25] employed a gradient recovery as the error estimate to solve MHD equations.

Comparatively, the adaptive element-free Galerkin technique based on element residual error has not received much investigation, even though it can provide quantifiable

Manuscript received March 18, 2022; revised October 21, 2022.

Min Wang is a doctoral candidate of the College of Civil Engineering & Architecture, China Three Gorges University, Yichang 443002, China (e-mail: wangmin@ctgu.com).

Gang Peng is a professor of the Civil Engineering & Architecture, China Three Gorges University, Yichang 443002, China (e-mail: gpeng158@126.com)

\*Xiaohua Zhang is an associate professor of the Three Gorges Mathematical Research Center, China Three Gorges University, Yichang 443002, China (corresponding author to provide phone: +8615872481386; e-mail: zhangxiaohua07@163.com)

information about the error. The high overlap support domain in most EFG making the calculation of residual function is complex. Another major obstacle is that in the new iterative step of the adaptive EFG process, with the change of node configuration, the support domain of each Gaussian integral point must be modified, and the shape function and its derivatives must be recalculated. Scholars have explored a variety of strategies to overcome this limitation, but to the authors' knowledge, not many studies have been done, except for Liu and Tu [29] proposed a residual method based on background cells and Afshar et al. [30] presented a node enrichment adaptive refinement in DLSSM.

As mentioned, the residual-based type method is carried out directly in integration elements, making it appropriate for analysis using the finite element approach and has obtained fruitful research findings. Zhang et al. tried to transplant some mature technologies of FEM into the EFG method by the so-called arbitrary convex polygonal influence domain technique [31] and gained some desirable results for the Poisson equation under the first boundary condition [32]. Inspired by these studies and to improve the method and extend its application, we focused on developing this adaptive EFG method and applying it to elasticity problems with mixed boundary conditions in this article.

The paper is structured as follows: Section II introduces some basic equations about the improved MLS approximation for the elastic problem. Section III details the process of applying adaptive analysis. Section IV demonstrates the application of the method to four numerical examples. Section V gives some conclusions about this method.

## II. ELEMENT FREE GALERKIN METHOD

The EFG method, like other numerical methods, establishes the shape function and combines it with the variational formulation of the governing problem to obtain the approximation of the solution. In particular, the variational equation is addressed in Galerkin weak form, and the shape function is constructed using the moving least square (MLS) technique.

### A. The MLS technique

The approximation function  $u^h(\mathbf{x})$  is written as follows:

$$u^h(\mathbf{x}) = \mathbf{p}^T(\mathbf{x}) \boldsymbol{\lambda}(\mathbf{x}) \quad (1)$$

where the  $\mathbf{p}^T(\mathbf{x})$  is the basis function and the coefficient vector  $\boldsymbol{\lambda}(\mathbf{x})$  is to be determined by the moving least-square (MLS) technique.

In 2-D problems, the most common linear basis is:

$$\mathbf{p}^T(\mathbf{x}) = [1, x, y] \quad (2)$$

And the frequently used quadratic basis is:

$$\mathbf{p}^T(\mathbf{x}) = [1, x, y, xy, x^2, y^2] \quad (3)$$

According to the MLS theory, at any point  $\mathbf{x}$ , the coefficient vector  $\boldsymbol{\lambda}(\mathbf{x})$  is obtained from the minimum weighted norm as follows:

$$\mathbf{J} = \sum_{i=1}^n w(\mathbf{x}, \mathbf{x}_i) [u^h(\mathbf{x}_i) - u_i]^2 \quad (4)$$

where  $n$  is the number of points in the influence domain of  $\mathbf{x}$ , and  $u_i$  is the nodal value of  $u$  at  $\mathbf{x} = \mathbf{x}_i$ . The most essential

part is the weight function  $w(\mathbf{x}, \mathbf{x}_i)$ , which indicates the contribution of each point in the influence domain of  $\mathbf{x}$ .

The stationarity of  $\mathbf{J}$  with respect to  $\boldsymbol{\lambda}(\mathbf{x})$  leads to the solution

$$\boldsymbol{\lambda}(\mathbf{x}) = \mathbf{A}^{-1}(\mathbf{x}) \mathbf{B}(\mathbf{x}) \mathbf{u} \quad (5)$$

where

$$\mathbf{A}(\mathbf{x}) = \sum_{i=1}^n w(\mathbf{x} - \mathbf{x}_i) \mathbf{p}(\mathbf{x}_i) \mathbf{p}^T(\mathbf{x}_i) \quad (6)$$

$$\mathbf{B}(\mathbf{x}) = [w(\mathbf{x} - \mathbf{x}_1) \mathbf{p}(\mathbf{x}_1), \dots, w(\mathbf{x} - \mathbf{x}_n) \mathbf{p}(\mathbf{x}_n)] \quad (7)$$

$$\mathbf{u} = [u(\mathbf{x}_1), u(\mathbf{x}_2), \dots, u(\mathbf{x}_n)]^T \quad (8)$$

Substituting Eq.(5) back into Eq.(1), the MLS approximation is expressed as

$$u^h(\mathbf{x}) = \mathbf{p}^T(\mathbf{x}) \mathbf{A}^{-1}(\mathbf{x}) \mathbf{B}(\mathbf{x}) \mathbf{u} = \boldsymbol{\Phi}^T \mathbf{u} \quad (9)$$

where  $\boldsymbol{\Phi}^T = \mathbf{p}^T(\mathbf{x}) \mathbf{A}^{-1}(\mathbf{x}) \mathbf{B}(\mathbf{x})$  is the shape function of EFG method.

In the EFG method, the support domain of the Gauss quadrature point has to be determined first. The next step is to calculate the shape function of each meshless node included in the influence domain. In contrast, the shape functions in the finite element method are produced directly from the meshed elements.

From the representation of Eq.(9), the approximate value at an arbitrary node  $\mathbf{x}^*$  can be expressed as  $u^h(\mathbf{x}^*) = \boldsymbol{\Phi}^T(\mathbf{x}^*) \mathbf{u} = \sum_{i=1}^n \Phi_i(\mathbf{x}^*) u(\mathbf{x}_i)$ , with  $u(\mathbf{x}_i)$  denoting the node value, and  $\Phi_i(\mathbf{x}^*)$  presenting the value of the corresponding shape function.

In general, unlike the FEM, the interpolation of MLS shape function of EFG is not available at field nodes, i.e.,  $\Phi_i(\mathbf{x}_j) \neq \delta_{ij}$ . Therefore, setting boundary conditions requires the use of other technique. The commonly used methods are: the Lagrange multiplier method [2], the direct collocation method [33], the penalty method [34], and the arbitrary convex polygonal influence domain technique [31] [35], etc.

The definition of influence domain plays a crucial role in the EFG method, as it determines the nodes contained in it. Although a circle or a rectangle would typically be chosen, this paper adopts the arbitrary convex polygonal influence domain technique

Start with the weighting function to demonstrate this method. For all instances in this work, the weighting function is the broadly used cubic spline function, as shown in the following:

$$w(\mathbf{x}, \mathbf{x}_i) = w(s) = \begin{cases} \frac{2}{3} - 4s^2 + 4s^3 & \text{if } s \leq \frac{1}{2} \\ \frac{4}{3} - 4s + 4s^2 - \frac{3}{4}s^3 & \text{if } \frac{1}{2} < s < 1 \\ 0 & \text{if } s \geq 1 \end{cases} \quad (10)$$

The weight parameter  $s$  is introduced to normalize the distance between  $\mathbf{x}$  and node  $\mathbf{x}_i$  in 2-D and 3-D problems.

When the influence domain is rectangular, the weight function of a 2-D problem is usually divided into horizontal and vertical directions as follows:

$$w(\mathbf{x}, \mathbf{x}_i) = w(s) = w(s_x) w(s_y) \quad (11)$$

where  $s_x = d_x/r_x$  and  $s_y = d_y/r_y$ , in which  $r_x$  and  $r_y$  indicate the corresponding influence distance of the neighborhood.

However, in the arbitrary convex polygonal influence domain technique, the variable  $s$  is modified as  $s_i = d_i/r(\theta)$ , which have different values at different angles  $\theta$  of the influence domain. Fig.1 shows the diagrammatic sketch of meshless node  $x_i$  with a convex polygonal influence domain ABCDE. Triangles  $\Delta x_i A' B'$ ,  $\Delta x_i B' C'$ ,  $\Delta x_i C' D'$ ,  $\Delta x_i D' E'$  and  $\Delta x_i E' A'$  are background integration cells covered by the influence domain ABCDE.

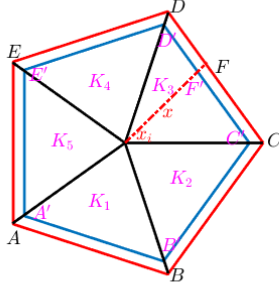


Fig. 1: Schematic diagram of convex polygonal influence region of node  $x_i$ .

Taken triangle  $\Delta x_i C' D'$ , in Fig.1 as the integration cell, where  $x$  is a point within the triangle (often the Gaussian point) [31]. The following steps sketch the construction of the shape function:

- Scale up the integration element to obtain the influence domain.
- Express the influence radius as  $r(\theta) = |x_i F| = \alpha |x_i F'|$  in the direction of  $\overrightarrow{x_i F}$ , with  $\alpha$  denoting the scale factor.
- Obtain  $r_x$  and  $r_y$  from the projected length of  $\overrightarrow{x_i F}$ .
- Compute the weight function value  $w(s)$  from Eq.(11) by the obtained  $r_x$  and  $r_y$ .
- Calculate the  $\Phi(x)$  of point  $x$  expressed as Eq.(9).

The influence domain parameter  $\alpha$  obeys different selection criteria in different EFG methods. Specifically, the scale factor is given as  $\alpha = 1.01$  in this paper.

The interpolation property of MLS shape function is preserved by the special value of  $\alpha$ , making it easier to impose essential boundary constraints. Furthermore, the Gaussian product point is directly influenced by the triangle containing it as this arbitrary convex polygonal impact domain technique is used [31]. Therefore, the EFG calculation time will be reduced significantly, moreover, the bandwidth of the system equations is minimized due to the smaller overlapping range of influence domains, allowing for more efficient calculations. Crucially, it can further simplify the process of the adaptive analysis in the EFG, which will be explained in detail in Section III.

On the approximation theory of MLS, Li [36] gave the following results in  $n$ -dimensional spaces.

**Theorem 1.** Assume that  $u(x) \in W^{p+1,q}(\Omega)$  with  $p+1 \geq \frac{n}{q}$  if  $q > 1$ , or  $p+1 \geq n$  if  $q = 1$ , where  $W^{p+1,q}(\Omega)$  is the

Sobolev space of functions defined on  $\Omega$ . Let  $u^h(x)$  given by Eq.(9) be the MLS approximation of  $u(x)$ , then there is a constant  $C$  independent of  $h$  such that

$$\|u(x) - u^h(x)\|_{W^{k,q}(\Omega)} \leq Ch^{\tilde{p}-k} \|u(x)\|_{W^{\tilde{p},q}(\Omega)} \quad (12)$$

$$k = 0, 1, \dots, \min\{\tilde{p}, \gamma\}, \quad \tilde{p} = \min\{p+1, \hat{m}+1\}.$$

Particularly, when  $u(x) \in W^{\hat{m}+1,q}(\Omega)$ , namely  $p \geq \hat{m}$ , we have

$$\|u(x) - u^h(x)\|_{W^{k,q}(\Omega)} \leq Ch^{\hat{m}+1-k} \|u(x)\|_{W^{\hat{m}+1,q}(\Omega)} \quad (13)$$

$$k = 0, 1, \dots, \min\{\hat{m}+1, \gamma\}$$

Besides, when  $u(x) \in H^{\hat{m}+1}(\Omega)$ , namely  $p \geq \hat{m}$  and  $q = 2$ , we have

$$\|u(x) - u^h(x)\|_{H^k(\Omega)} \leq Ch^{\hat{m}+1-k} \|u(x)\|_{H^{\hat{m}+1}(\Omega)} \quad (14)$$

$$0 \leq k \leq \min\{\hat{m}+1, \gamma\}$$

### B. The global weak form for linear elastic problems

The equilibrium equation of elastic problem is as follows:

$$\nabla \cdot \boldsymbol{\sigma} + \mathbf{b} = \mathbf{0} \text{ in } \Omega \quad (15)$$

where  $\Omega$  is bounded by  $\Gamma$ ,  $\boldsymbol{\sigma}$  is the stress vector, and  $\mathbf{b}$  is the body force vector.

The mixed boundary conditions are usually described as:

$$\mathbf{u} = \bar{\mathbf{u}} \text{ on } \Gamma_u, \quad (16)$$

$$\boldsymbol{\sigma} \cdot \mathbf{n} = \bar{\mathbf{t}} \text{ on } \Gamma_t.$$

where  $\bar{\mathbf{u}}$  presents the constraint displacement on the boundary  $\Gamma_u$ ,  $\bar{\mathbf{t}}$  is the imposed traction on the boundary  $\Gamma_t$ , and  $\mathbf{n}$  is the unit normal vector outward to  $\Gamma_t$ .

This governing equation, described with displacement  $\mathbf{u}$ , strain  $\boldsymbol{\varepsilon}$ , stress  $\boldsymbol{\sigma}$ , can be expressed by displacement forms, basing on the basic equations of 2-D elasticity mechanics:

$$\mathbf{u} = \{u_x, u_y\}^T, \quad (17)$$

$$\boldsymbol{\varepsilon} = \nabla \mathbf{u},$$

$$\boldsymbol{\sigma} = \mathbf{D} \boldsymbol{\varepsilon}.$$

where matrix  $\mathbf{D}$  describes the elasticity (constitutive) matrix.

For plane stress condition:

$$\mathbf{D} = \frac{E}{1-\nu^2} \begin{bmatrix} 1 & \nu & 0 \\ \nu & 1 & 0 \\ 0 & 0 & \frac{1-\nu}{2} \end{bmatrix}, \quad (18)$$

For plane strain condition:

$$\mathbf{D} = \frac{E}{(1-2\nu)(1+\nu)} \begin{bmatrix} 1-\nu & \nu & 0 \\ \nu & 1-\nu & 0 \\ 0 & 0 & \frac{1-2\nu}{2} \end{bmatrix}, \quad (19)$$

where  $E$  is the Young's modulus and  $\nu$  is the Poisson's ratio of the material.

For the convenience of expression, rendering nonhomogeneous boundary conditions to homogeneous form in a standardized way, the displacement boundary condition can be assumed to be homogeneous as:  $\bar{\mathbf{u}} = \mathbf{0}$ .

The Galerkin weak form of elastic problems is:

$$\int_{\Omega} \nabla \mathbf{u}^T \mathbf{D} \nabla \mathbf{v} d\Omega - \int_{\Omega} \mathbf{b}^T \mathbf{v} d\Omega - \int_{\Gamma_t} \bar{\mathbf{t}}^T \mathbf{v} d\Gamma = 0 \quad (20)$$

The global weak formulation for elastic problems is:

$$\begin{cases} \text{find } \mathbf{u} \in V & \text{such that} \\ a(\mathbf{u}, \mathbf{v}) = l(\mathbf{v}), \quad \forall \mathbf{v} \in V. \end{cases} \quad (21)$$

where  $a(\cdot, \cdot)$  is a continuous and coercive bilinear operator on  $V = \left\{ \mathbf{u} \in (H^1(\Omega))^2 : \mathbf{u}|_{\Gamma_u} = \mathbf{0} \right\}$

$$a(\mathbf{u}, \mathbf{v}) = \int_{\Omega} \nabla \mathbf{u}^T \mathbf{D} \nabla \mathbf{v} d\Omega \quad (22)$$

and

$$l(\mathbf{v}) = \int_{\Omega} \mathbf{b}^T \mathbf{v} d\Omega + \int_{\Gamma_t} \bar{\mathbf{t}}^T \mathbf{v} d\Gamma. \quad (23)$$

The approximation for the global Galerkin formulation would be:

$$\begin{cases} \text{find } \mathbf{u}^h \in V_h(\Omega) & \text{such that} \\ a(\mathbf{u}^h, \mathbf{v}^h) = l(\mathbf{v}^h), \quad \forall \mathbf{v}^h \in V_h(\Omega). \end{cases} \quad (24)$$

where  $V_h$  is the finite dimensional subspace generated by the EFG method, and it is a subspace of  $V$ , and the MLS approximation function  $\mathbf{u}^h(\mathbf{x})$  in Eq.(9) is utilized as the trial function to obtain the final discrete equations.

Substituting Eq.(9) into the approximate formulation Eq.(24), it generates the following system of linear equations:

$$\mathbf{K}\mathbf{u} = \mathbf{F} \quad (25)$$

where

$$\mathbf{u} = [\mathbf{u}_1, \mathbf{u}_2, \dots, \mathbf{u}_n]^T, \quad (26)$$

$$\mathbf{u}^h(\mathbf{x}) = \Phi^T(\mathbf{x}) \mathbf{u} = \sum_{i=1}^n \Phi_i(\mathbf{x}) \mathbf{u}_i \quad (27)$$

$$\mathbf{K}_{ij} = \int_{\Omega} \mathbf{B}_i^T \mathbf{D} \mathbf{B}_j d\Omega, \quad i, j = 1, 2, \dots, n, \quad (28)$$

$$\mathbf{F}_i = \int_{\Omega} \mathbf{b}^T \Phi_i d\Omega + \int_{\Gamma_t} \bar{\mathbf{t}}^T \Phi_i d\Gamma, \quad i = 1, 2, \dots, n, \quad (29)$$

with

$$\mathbf{B}_i = \begin{bmatrix} \Phi_{i,x} & 0 \\ 0 & \Phi_{i,y} \\ \Phi_{i,y} & \Phi_{i,x} \end{bmatrix}, \quad i = 1, 2, \dots, n \quad (30)$$

Cheng and Cheng [23] gave a priori error estimations results in the meshless method for elastic problems like the FEM as follows:

**Theorem 2.** Let  $\mathbf{u} \in V(\Omega)$  be the analytical solution of the boundary value problem Eq.(20), let  $\mathbf{u}_h \in V_h(\Omega)$  be the solution of the variational problem Eq.(24), then there is a constant  $C$  independent of mesh size  $h$  such that

$$\|\mathbf{u} - \mathbf{u}_h\|_1 \leq C \|\mathbf{u}\|_2 \quad (31)$$

where  $\|\cdot\|_1$  is the norm of space  $H^1$ , and  $\|\cdot\|_2$  is the norm of space  $H^2$ .

As the MLS shape function generated by this special influence domain almost exhibits interpolation properties, combining Schwarz inequality, Trace Theorem, Theorem 1, it can be proved simply that the result of Theorem 2 is applicable to the method of this paper.

### III. ADAPTIVE REFINEMENT ALGORITHM

Contrary to the uniform refinement, the adaptive refinement algorithm aims to refine only a few locations where the solution changes rapidly more than in the other regions. Error estimation and domain refining are therefore two crucial components of every adaptive analysis technique. In traditional adaptive meshfree analysis, the influence domains may be highly overlapping, which brings trouble to implement the two processes mentioned above, even to the new iteration step, the re-search of nodes falling into a support domain and the re-construction of shape functions of the corresponding searched nodes may be time-consuming.

However, in this EFG method, using triangular grid as the background integral elements and setting  $\alpha = 1.01$  can generate smaller overlapped influence domains and provide greater convenience for adaptive analysis. First, the Gauss quadrature point is only affected by the vertices of that triangular itself, and the shape function of this MLS method has the interpolation property, which is similar to those of the FEM, therefore element residual error estimation can be directly calculated and marked on the integration elements, and the mature posteriori estimator techniques of the FEM can be transplanted to the EFG method without much change. In addition, the refinement can be made directly on the background mesh, whereas most adaptive meshless methods have to refine the meshless nodes.

Let  $T_0$  be a conforming triangular background integrational mesh on the computational domain  $\Omega$ , and let  $\{T_k\}_{k>0}$  be the sequential local refinement background integrational meshes. The mesh  $T_{k+1}$  is generated from  $T_k$ . The adaptive procedure can be performed by iterating the following loop:

SOLVE  $\rightarrow$  ESTIMATE  $\rightarrow$  MARK  $\rightarrow$  REFINES

- Solve

Solving the given PDE by the introduced EFG method in Section II on the conforming triangular background mesh  $T_k$ .

- Estimate

Estimating the error over the integration cell is one of the critical components of the adaptive method. To obtain the indicators of each field node required by the subsequent module, the posteriori error estimator is widely used. There are two kinds of a posteriori error estimator broadly used in the FEM: one is the recovery-based methods, the other is the residual-based methods. Both have rich theoretical results and practical experience in adaptive analysis, but the latter is still rarely studied in the general EFG method.

The error estimation used in this paper is similar to a widely used standard element residual technique in the FEM [37]. The element residual  $\eta_k$  used in this paper is defined as:

$$\eta_k = h_k \|\mathbf{f} + \nabla \sigma_h\|_K + h_K^{\frac{1}{2}} \left( \frac{1}{2} \|\sigma_h \cdot \mathbf{n}\|_{\partial K \setminus \partial \Omega} + \|\bar{\mathbf{t}} - \sigma_h \cdot \mathbf{n}\|_{\partial K \cap \Gamma_t} \right) \quad (32)$$

where  $h_k \|\mathbf{f} + \nabla \sigma_h\|_K$  is the cell residual and the rest part represents the edge residual.

- Mark

After getting the error indicator, the following procedure is to decide which background integration elements need

to be improved, which is named as the mark module. Generally, some user-defined criteria are given in advance. If the value on the edge of the background integration element or the value of the background integration element itself is greater than the given value, these elements should be marked and refined at the subsequent process.

We adopt the Dörfler's bulk marking strategy to mark the key areas in this paper, which is one of the widely used adaptive FEM marking strategies.

Firstly, let  $\eta_k$  denotes the error factor of each triangular background integration  $k$ . The global error is calculated by adding together all the element errors as:

$$\eta^2 = \sum_{k \in T_k} \eta_k^2 \quad (33)$$

Then, identify a certain subset  $M \subset T_k$  by a user-defined marking parameter  $\theta$ :

$$\theta \eta^2 = \sum_{\tau \in M} \eta_\tau^2 \quad (34)$$

where  $\theta \in (0, 1]$ . The mesh density decreases as the value  $\theta$  increases.

- Refine

In this paper, bisecting the marked triangular background integration cells to achieve the refinement [17]. There are many details about the "newest vertex bisection" technique in [20].

#### IV. NUMERICAL RESULTS AND DISCUSSION

The efficiency of this proposed adaptive method is verified by four elastic problems. These benchmark problems discussed in this section are classic examples of adaptive procedure testing, as they are either highly concentrated in some areas or have stress singularities in special regions.

In this paper, a triangular mesh is used as the background integration element, the linear basis is selected in the MLS method, and the element-based Dörfler labeling strategy is used to execute the adaptive EFG algorithm, letting the marking parameter  $\theta = 0.4$ .

##### A. Cantilever beam

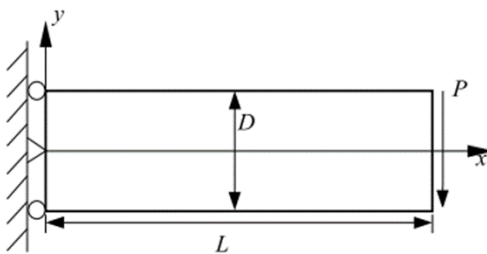


Fig. 2: Cantilever beam loaded at the free edge.

As shown in Fig.2, a unit thickness cantilever beam is loaded at the free edge. The material of the beam is elastic, with Young's modulus  $E = 3.0 \times 10^7$  and Poisson's ratio  $\nu = 0.3$ . The length and width of the beam are  $L = 48$  and  $D = 12$ . A distributed shear force  $P = 1000$  is imposed at the right edge and a displacement constrained  $u_x = 0$

is applied at the left edge. The exact solution is given by Timoshenko and Goodier [38] as follows:

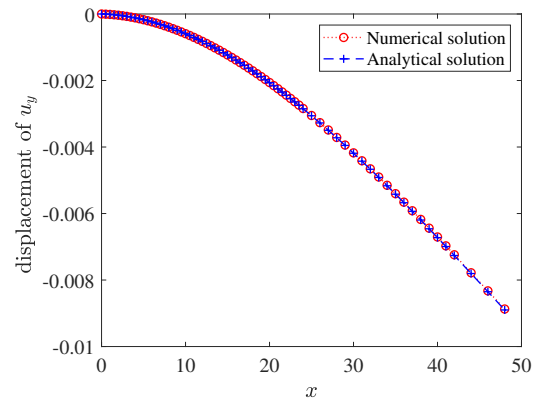
$$\begin{aligned} u_x &= -\frac{Py}{6EI} \left[ (6L - 3x)x + (2 + \nu) \left( y^2 - \frac{1}{4}D^2 \right) \right] \\ u_y &= \frac{P}{6EI} \left[ 3\nu y^2 (L - x) + \frac{1}{4}D^2 (4 + 5\nu)x + (3L - x)x^2 \right] \end{aligned} \quad (35)$$

for displacements, and

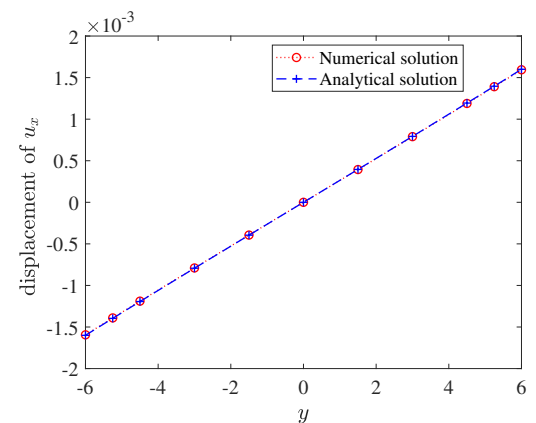
$$\begin{aligned} \sigma_{xx} &= -\frac{P(L-x)y}{I}, \\ \sigma_{yy} &= 0, \\ \sigma_{xy} &= \frac{P}{2I} \left( \frac{D^2}{4} - y^2 \right). \end{aligned} \quad (36)$$

for stresses, where  $I = \frac{D^3}{12}$  is the cantilever moment of inertia.

The analytical solution indicates stress concentrating at the fixed left end, and we'd better place rich enough nodes near this area. In this paper,  $13 \times 5$  nodes are uniformly arranged initially; the stopping condition is determined by the final number of nodes or the steps of refinement.



(a) Vertical displacement along the central line



(b) Horizontal displacement on the right edge

Fig. 3: Displacement of the cantilever beam.

The results for this loaded beam are shown in Fig.3-Fig.7. Fig.3-Fig.5 show that the numerical results consistent with the analytical solutions. The distribution of the final nodes of our adaptive algorithm is shown in Fig.6, it reveals that the refinement is carried out on the constrained boundary where the stress concentration occurs. The a posteriori error

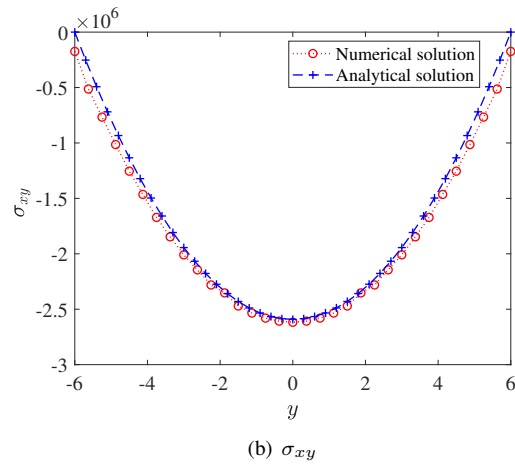
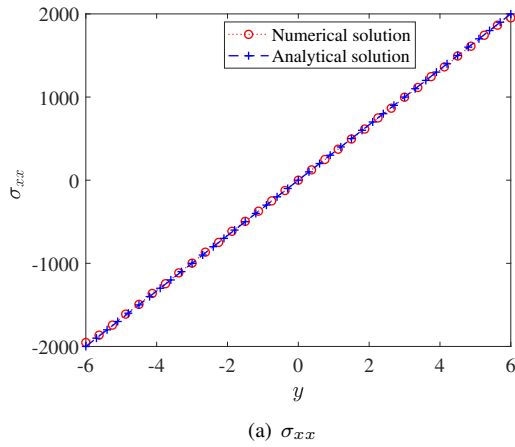


Fig. 4: Stresses along left end of the cantilever beam.

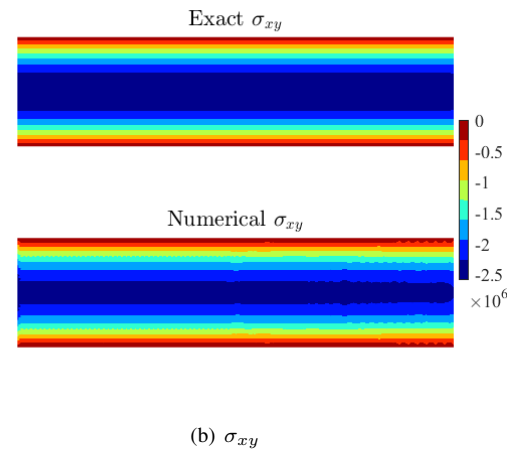
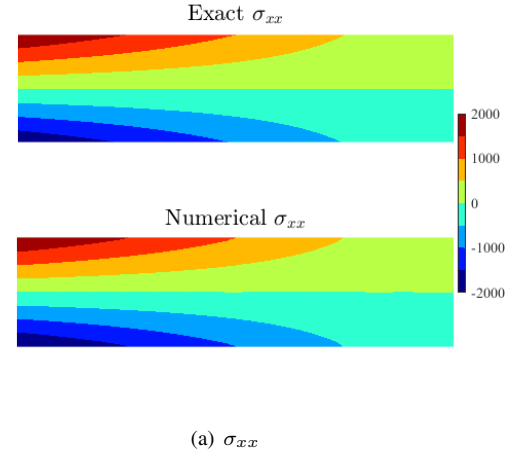


Fig. 5: Contours of stresses with 25 adaptive steps and the exact solution.

estimates' convergence is displayed in Fig.7. Estimates of errors decline monotonically at a rate of  $\mathcal{O}(N^{-0.51})$ , which is almost identical to the optimal rate of the linear adaptive finite element method, where  $N$  is the total number of nodes for each adaptive step.

### B. An infinite plate with a circular hole

As shown in Fig.8, an infinite plate that has a hole in the middle is affected by a uniaxial tension  $P$ .

The analytical solution of displacements and stresses of this problem are given by Timoshenko and Goodier [38] in the polar coordinates  $(r, \theta)$  as:

$$\begin{aligned} u_x &= \frac{Pa}{8G} \left( \frac{r}{a} (1 + \kappa) \cos \theta + \frac{2a}{r} ((1 + \kappa) \cos \theta + \cos 3\theta) - \frac{2a^3}{r^3} \cos 3\theta \right) \\ u_y &= \frac{Pa}{8G} \left( \frac{r}{a} (\kappa - 3) \sin \theta + \frac{2a}{r} ((1 - \kappa) \sin \theta + \sin 3\theta) - \frac{2a^3}{r^3} \sin 3\theta \right) \end{aligned} \quad (37)$$

$$\begin{aligned} \sigma_{xx} &= \frac{P}{2} \left( 2 - \frac{a^2}{r^2} \left( 3 \cos 2\theta + \left( 2 - 3 \frac{a^2}{r^2} \right) \cos 4\theta \right) \right) \\ \sigma_{yy} &= -\frac{Pa^2}{2r^2} \left( \cos 2\theta - \left( 2 - 3 \frac{a^2}{r^2} \right) \cos 4\theta \right) \\ \tau_{xy} &= -\frac{Pa^2}{2r^2} \left( \sin 2\theta - \left( 2 - 3 \frac{a^2}{r^2} \right) \sin 4\theta \right) \end{aligned} \quad (38)$$

where  $a$  is the hole radius,  $\nu$  is the Poisson's ratio,  $G =$

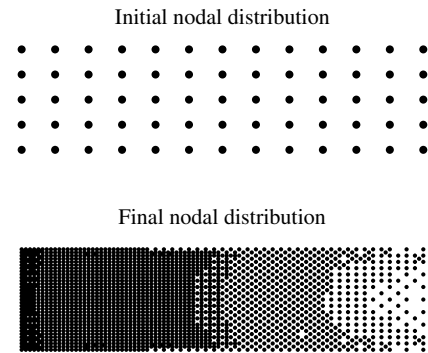


Fig. 6: Node distribution of cantilever beam loaded at the free end.

is the shear modulus, and Kolosov constant is:

$$\kappa = \begin{cases} \frac{3-\nu}{1+\nu} & \text{for plane stress} \\ 3-4\nu & \text{for plane strain} \end{cases} \quad (39)$$

The problem domain for numerical modeling is a bounded square zone with side lengths substantially longer than the hole's radius. Usually, only the first quadrant of the plate is examined due to symmetry. In this work, assume that the length of the edge to be analyzed is  $5a$ .

This problem is considered as a plane stress problem. The left edge is fixed horizontally, while the bottom edge is fixed vertically. The right and upper edges are subjected

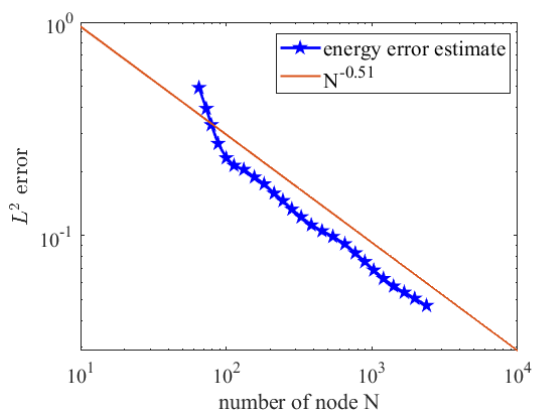


Fig. 7: Error estimation of the adaptive algorithm for the cantilever beam.

to the traction converted from the uniaxial tension. Suppose Young's modulus  $E = 1000$ , Poisson's ratio  $\nu = 0.3$ , and the tension  $P = 1000$ .

Fig.9-10 show that the numerical results agree well with the analytical solutions. The initial nodal configuration and the last adapted configuration shown in Fig.11 indicate distinctly that the point density is higher around the regions with a significantly changed solutions. Fig.12 demonstrates the convergence of this proposed error estimation, and the decay rate of error estimates is  $\mathcal{O}(N^{-0.49})$ , with  $N$  denoting the total number of nodes in each adaptive step.

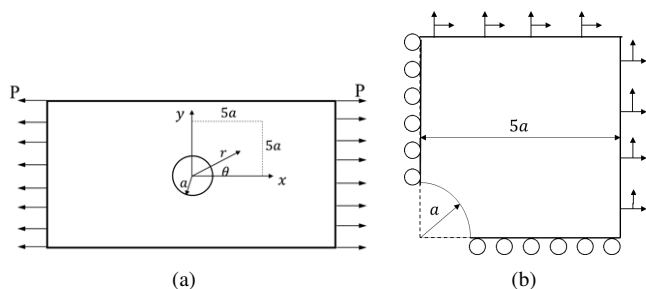


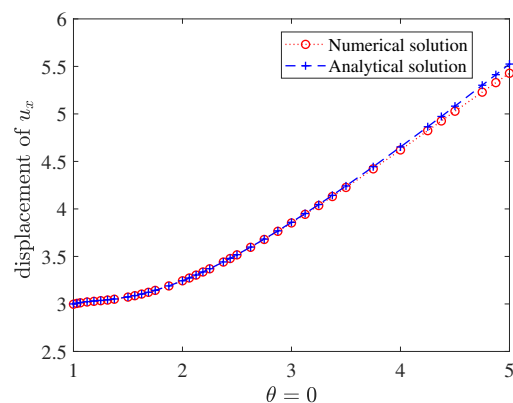
Fig. 8: An infinite plate with a circular hole subjected a uniaxial tension  $P$ .

### C. An Edge-cracked Rectangular Body Subject to Tension

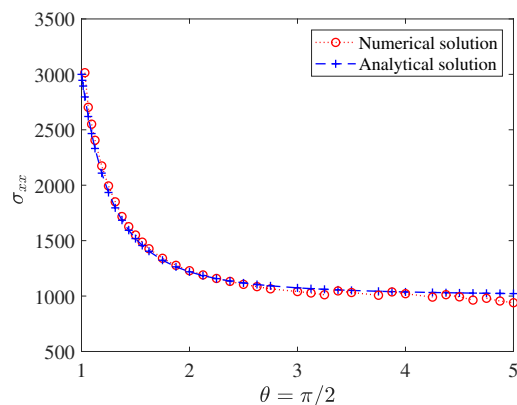
A rectangle plate with an edge-cracked is shown in Fig.13. Let  $a = 4$ ,  $L = 20$ ,  $D = 26$ , material constants of Young's modulus  $E = 2.0 \times 10^5$  and Poisson's ratio  $\nu = 0.25$ . The rectangle plate is under a uniform tension  $P = 1$  in the vertical direction at the upper and bottom ends. This example is a typical Griffith mode-I crack problem. The analytic solution at the crack tip is given by Anderson [39] in the polar coordinates  $(r, \theta)$  as:

$$\begin{aligned} \sigma_{xx} &= \frac{K_I}{\sqrt{2\pi r}} \cos \frac{\theta}{2} \left(1 - \sin \frac{\theta}{2} \sin \frac{3\theta}{2}\right) \\ \sigma_{yy} &= \frac{K_I}{\sqrt{2\pi r}} \cos \frac{\theta}{2} \left(1 + \sin \frac{\theta}{2} \sin \frac{3\theta}{2}\right) \\ \tau_{xy} &= \frac{K_I}{\sqrt{2\pi r}} \cos \frac{\theta}{2} \sin \frac{\theta}{2} \sin \frac{3\theta}{2} \end{aligned} \quad (40)$$

where the stress intensity factor  $K_I$  is prescribed by  $K_I = P\sqrt{\pi a}$ .



(a) Horizontal displacement along  $y = 0$



(b) Normal stress  $\sigma_{xx}$  along  $x = 0$ .

Fig. 9: Comparison between numerical solution and analytical solution .

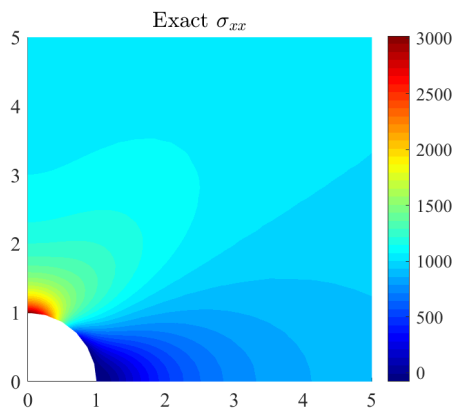
A conventional way is to calculate the top half of the plate, on account of symmetry. Results concerned with this example are shown in Fig.14–Fig.16.

The coherence between the computing results with the exact solution in Fig.14 indicates that the method in the paper is reliable. Fig.15 depicts that, as expected, after the performance of this adaptive method, the majority of nodes are distributed around the crack tip, where the stress singularity happened. Fig.16 displays the convergence for the a posteriori error estimates. Estimates of errors decline monotonically at a rate of  $\mathcal{O}(N^{-0.51})$ , where  $N$  denotes the total number of nodes in each adaptive step.

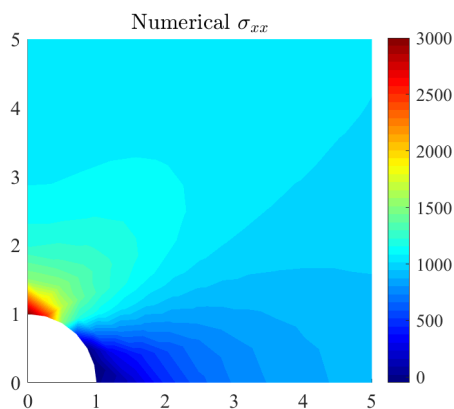
### D. L-shaped plate

The fourth example concerns an  $L$ -shaped plate under the transverse loads, as illustrated in Fig.17 with  $a = 25$ , material constants as Young's modulus  $E = 3.0 \times 10^7$  and Poisson's ratio  $\nu = 0.3$ . A unit traction  $P$  is applied at the right edge. The left edge is fixed horizontally, while the bottom edge is fixed vertically. This problem is a standard test case for the refining processes, because the stress at the inner corner of the plate is singular.

As Fig.18 reveals, the refinement is assembled around the corner point, despite the initial nodes are uniformly distributed. The contours of stress  $\sigma_{xx}$  with different adaptive steps shown in Fig.19 demonstrate obviously that the maximum stress increasing with the proceeding of adaptivity. These indicate that the interior corner of the plate is the



(a)



(b)

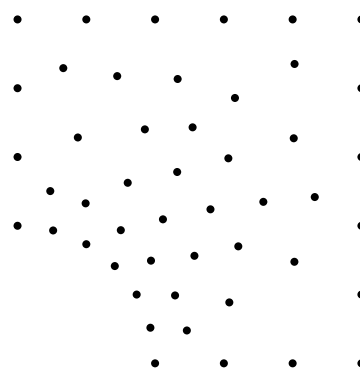
Fig. 10: Contours of stresses with 25 adaptive steps and the exact solution.

stress singularity point, and the expected refinements are implemented near the point. The a posteriori error estimates' convergence is demonstrated in Fig.20. Estimates of errors decline monotonically at a rate of  $\mathcal{O}(N^{-0.47})$ , where  $N$  denotes the total number of nodes in each adaptive step.

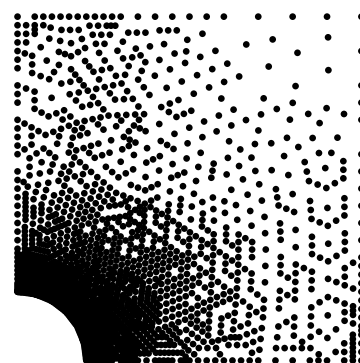
V. CONCLUSION

An interpolation h-refinement procedure of element free Galerkin method is proposed to solve some elastic problems. This approach takes full benefit of the meshless method and the adaptive finite element method by transferring proven and effective adaptive techniques from FEM directly into EFG. Instead of most recovery-based adaptive EFG methods, this method uses residual-based error estimation as the refinement metric. The particular value of the scalar factor  $\alpha$  of the special influence domain not only gives interpolation property to the shape function of the EFG method but also makes it possible to use a refinement similar to that of the adaptive finite element method. One of the broadly used residual error estimation of the AFEM is taken as the EFG error estimation strategy in this paper.

The adaptive interpolation element free Galerkin method for Poisson equation with Dirichlet boundary conditions is extended to linear elastic problems of mixed boundary conditions and the desired results are obtained. The numerical results of four benchmark problems demonstrate the validity and efficiency of the proposed adaptive EFG



(a) Initial nodal distribution



(b) Final nodal distribution.

Fig. 11: Node distribution of an infinite plate with a circular hole.

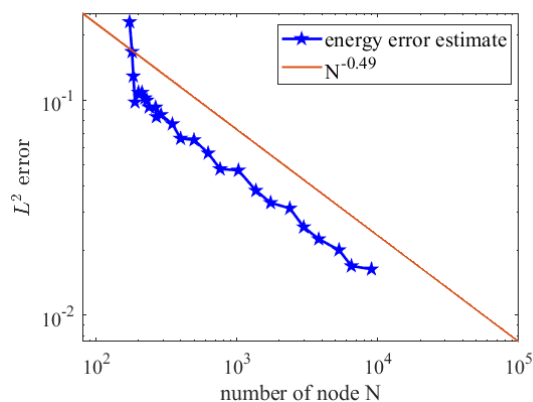


Fig. 12: Error estimates of the adaptive algorithm employing for an infinite plate with a circular hole.

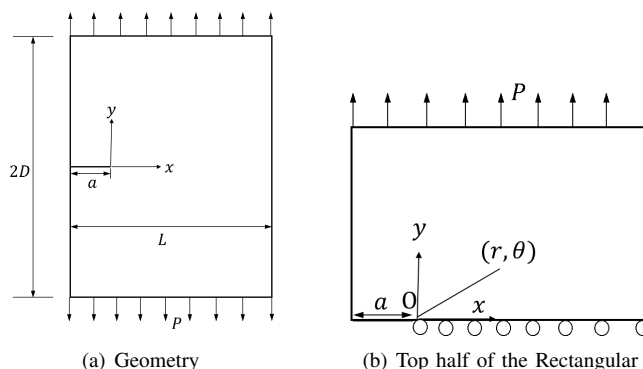


Fig. 13: An Edge-cracked Rectangular Body Subject to Tension.



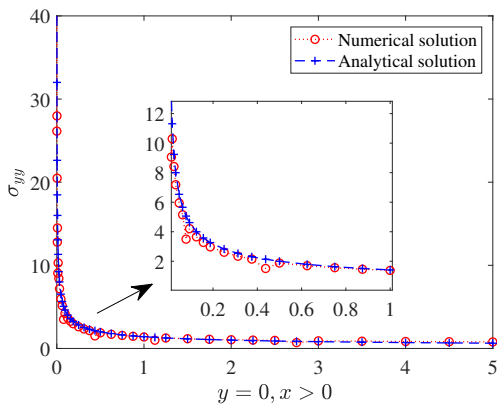


Fig. 14: Normal stress  $\sigma_{yy}$  along the right hand of the crack-tip, where  $\theta = 0$ .

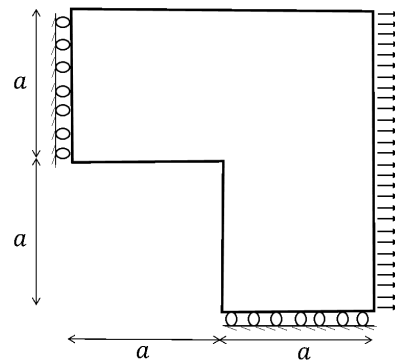
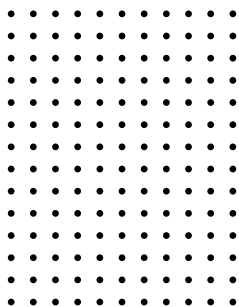
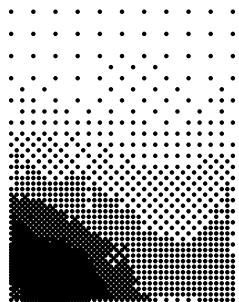


Fig. 17: L shape plate subjected to a uniform tension



(a) Initial nodal distribution



(b) Final nodal distribution.

Fig. 15: Node distribution of an edge-cracked rectangular body subject to tension.

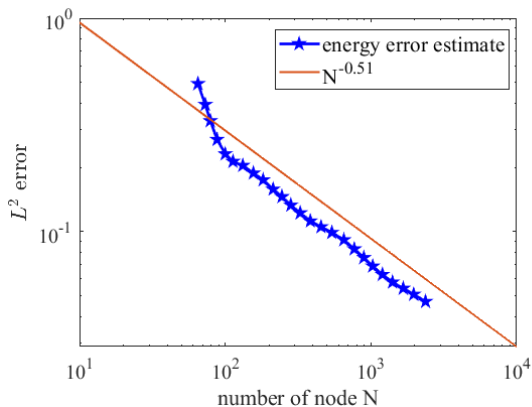
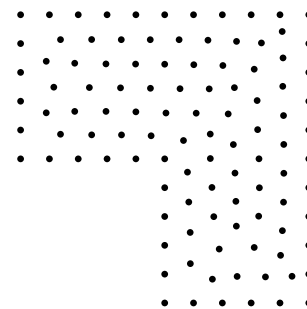
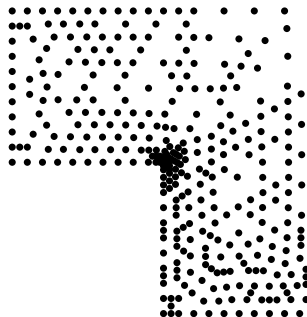


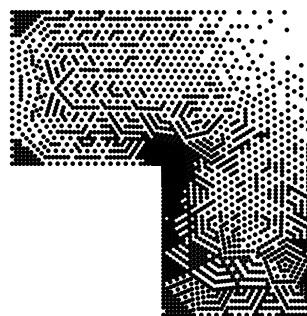
Fig. 16: Error estimates of the adaptive algorithm employing for an edge-cracked rectangular body subject to tension



(a) Initial nodal distribution

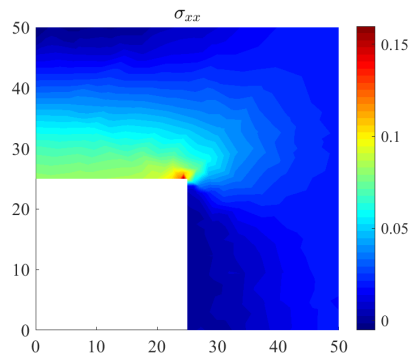


(b) Nodal distribution with 7 adaptive steps

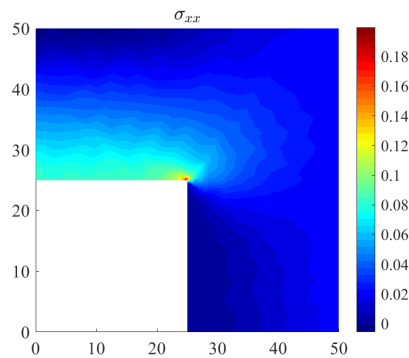


(c) Final nodal distribution with 16 adaptive steps.

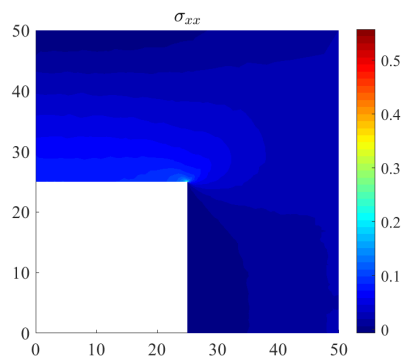
Fig. 18: Nodal distribution of the L-shaped plate with different adaptive steps.



(a) Stress  $\sigma_{xx}$  with 4 adaptive steps.



(b) Stress  $\sigma_{xx}$  with 7 adaptive steps.



(c) Stress  $\sigma_{xx}$  with 16 adaptive steps.

Fig. 19: Contours of  $\sigma_{xx}$  of the L-shaped plate with different adaptive steps.

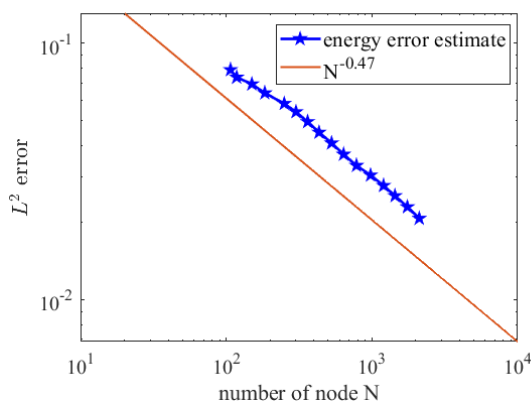


Fig. 20: Error estimates of the adaptive algorithm employing for the L-shaped plate.

method. As expected, the refinements are around the regions with drastically varying gradients and discontinuities, and the convergence of this adaptive analysis is almost consistent with the optimal rate of the finite method. In the future, we will investigate the method's application in non-linear and dynamic problems.

REFERENCES

- [1] T. Belytschko, L. Gu and Y. Y. Lu, "Fracture and crack growth by element free Galerkin methods," *Modelling and Simulation in Materials Science and Engineering*, vol. 2, no. 3A, pp. 519-534, 1994.
- [2] T. Belytschko, Y. Krongauz and D. Organ and M. Fleming and P. Krysl, "Meshless method: An overview and recent development," *Computer Methods in Applied Mechanics and Engineering*, vol. 139, no. 1, pp. 3-47, 1996.
- [3] T. Belytschko, Y. Y. Lu and L. Gu, "Element-free Galerkin methods," *International Journal for Numerical Methods in Engineering*, vol. 37, no. 2, pp. 229-256, 1994.
- [4] J. S. Chen, M. Hillman and S. W. Chi, "Meshfree methods: Progress made after 20 years," *Journal of Engineering Mechanics*, vol. 143, no. 4, pp. 04017001-38, 2017.
- [5] V. G. Patel and N. V. Rachchh, "Meshless method-review on recent developments," *Materials today: proceedings*, vol. 26, pp. 1598-1603, 2020.
- [6] T. Sun and R. Zheng, "An upwind-mixed finite element method with moving grids for quasi-nonlinear Sobolev equations," *IAENG International Journal of Applied Mathematics*, vol. 47, no. 4, pp. 465-470, 2017.
- [7] Y. Belaasilia, A. Timesli, B. Braikat and M. Jamal, "A numerical mesh-free model for elasto-plastic contact problems," *Engineering Analysis with Boundary Elements*, vol. 82, pp. 68-78, 2017.
- [8] S. H. Lee and Y. C. Yoon, "An improved crack analysis technique by element-free Galerkin method with auxiliary supports," *International Journal for Numerical Methods in Engineering*, vol. 56, no. 9, pp. 1291-1314, 2003.
- [9] P. Profifizi, A. Combescure and K. Ogawa, "SPH modeling of adhesion in fast dynamics: Application to the cold spray process," *Comptes Rendus Mecanique*, vol. 344, no. 4, pp. 211-224, 2016.
- [10] G. R. Liu and Y. T. Gu, *An Introduction to Meshfree Methods and Their Programming*. Dordrecht, Netherland: Springer, 2005.
- [11] H. G. Kwak and J. W. Hwang, "Non-linear finite element analysis of a steel-concrete composite beam under cyclic loads considering interface slip effects," *Engineering Letters*, vol. 19, no. 3, pp. 249-254, 2011.
- [12] J. L. Yan and Z. Y. Zhang, "Two-grid methods for characteristic finite volume element approximations of semi-linear Sobolev equations," *Engineering Letters*, vol. 23, no. 3, pp. 189-199, 2015.
- [13] D. W. Kelly, J. P. De, S. R. Gago and O. C. Zienkiewicz, "A posteriori error analysis and adaptive processes in the finite element method: Part I-error analysis," *International Journal for Numerical Methods in Engineering*, vol. 19, no. 11, pp. 1593-1619, 1983.
- [14] O. C. Zienkiewicz and J. Z. Zhu, "A simple error estimator and adaptive procedure for practical engineering analysis," *International Journal for Numerical Methods in Engineering*, vol. 24, no. 2, pp. 337-357, 1987.
- [15] J. T. Oden, L. Demkowicz, W. Rachowicz and T. A. Westermann, "Toward a universal h-p adaptive finite element strategy, part 2. a posteriori error estimation," *Computer Methods in Applied Mechanics and Engineering*, vol. 77, no. 1-2, pp. 113-180, 1989.
- [16] R. H. Nochetto, K. G. Siebert and A. Veiser, *Theory of adaptive finite element methods: An introduction*. Germany: Springer Berlin Heidelberg, 2009.
- [17] C. Liu, L. Zhong, S. Shi and Y. Xiao, "Quasi-optimal complexity of adaptive finite element method for linear elasticity problems in two dimensions," *Applied Mathematics and Mechanics (English Edition)*, vol. 37, no. 2, pp. 151-168, 2016.
- [18] M. Ainsworth and J. Oden, "A posteriori error estimation in finite element analysis," *Computer Methods in Applied Mechanics and Engineering*, vol. 142, no. 1, pp. 1-88, 1997.
- [19] O. C. Zienkiewicz and J. Z. Zhu, "The superconvergent patch recovery and a posteriori error estimates. part 2: Error estimates and adaptivity," *International Journal for Numerical Methods in Engineering*, vol. 33, no. 7, pp. 1365-1382, 1992.
- [20] R. Verfürth, *A posteriori error estimation techniques for finite element methods*. Oxford: Oxford University Press, 2013.
- [21] H. J. Chung and T. Belytschko, "An error estimate in the EFG method," *Computational Mechanics*, vol. 21, no. 2, pp. 91-100, 1998.

- [22] C. K. Lee and C. E. Zhou, "On error estimation and adaptive refinement for element free Galerkin method: Part I: Stress recovery and a posteriori error estimation," *Computers & Structures*, vol. 82, no. 4/5, pp. 413-428, 2004.
- [23] R. J. Cheng and Y. M. Cheng, "Error estimate of element-free Galerkin method for elasticity," *Acta Physica Sinica*, vol. 60, no. 7, pp. 1729-1736, 2011.
- [24] Y. He, H. Yang and A. J. Deeks, "A node-based error estimator for the element-free Galerkin (EFG) method," *International Journal of Computational Methods*, vol. 11, no. 4, pp. 13500591-24, 2014.
- [25] Z. Jannesari and M. Tatari, "Magnetohydrodynamics (MHD) simulation via an adaptive element free Galerkin method," *Engineering with Computers*, vol. 38, no. 1, pp. 679-693, 2022.
- [26] I. Hajjout, M. Haddouch and E. M. Boudi, "An h-adaptive element-free Galerkin meshless method using a posteriori error estimator," *Materials Today Communications*, vol. 25, pp. 1014681-14, 2020.
- [27] P. Metsis, N. Lantzounis and M. Papadrakakis, "A new hierarchical partition of unity formulation of EFG meshless methods," *Computer Methods in Applied Mechanics & Engineering*, vol. 283, pp. 782-805, 2015.
- [28] B. Kumar, M. Somireddy and A. Rajagopal, "Adaptive analysis of plates and laminates using natural neighbor Galerkin meshless method," *Engineering with Computers*, vol. 35, no. 1, pp. 201-214, 2019.
- [29] G. R. Liu and Z. H. Tu, "An adaptive procedure based on background cells for meshless methods," *Computer Methods in Applied Mechanics & Engineering*, vol. 191, no. 17-18, pp. 1923-1943, 2002.
- [30] M. H. Afshar, J. Amani, and M. Naisipour, "A node enrichment adaptive refinement in discrete least squares meshless method for solution of elasticity problems," *Engineering Analysis with Boundary Elements*, vol. 36, no. 3, pp. 385-393, 2012.
- [31] X. Zhang, P. Zhang, and L. Zhang, "An improved meshless method with almost interpolation property for isotropic heat conduction problems," *Engineering Analysis with Boundary Elements*, vol. 37, no. 5, pp. 850-859, 2013.
- [32] X. Zhang, Z. Hu and M. Wang, "An adaptive interpolation element free Galerkin method based on a posteriori error estimation of FEM for Poisson equation," *Engineering Analysis with Boundary Elements*, vol. 130, no. 1, pp. 186-195, 2021.
- [33] X. Zhang, X. Liu, K. Song and M. Lu, "Least-squares collocation meshless method," *International Journal for Numerical Methods in Engineering*, vol. 51, no. 9, pp. 1089-1100, 2001.
- [34] S. N. Atluri and T. Zhu, "A new meshless local Petrov-Galerkin (MLGP) approach in computational mechanics," *Computational Mechanics*, vol. 22, no. 2, pp. 117-127, 1998.
- [35] X. Cao and X. Zhang, "Variational multiscale element free Galerkin method for three-dimensional steady convection-diffusion problems," *IAENG International Journal of Applied Mathematics*, vol. 52, no. 2, pp. 391-403, 2022.
- [36] X. Li, "Error estimates for the moving least-square approximation and the element-free Galerkin method in n-dimensional spaces," *Applied Numerical Mathematics*, vol. 99, no. JAN., pp. 77-97, 2016.
- [37] A. Besspalov, L. Rocchi and D. Silvester, "T-IFISS: a toolbox for adaptive FEM computation," *Computers & Mathematics with Applications*, vol. 81, pp. 373-390, 2021.
- [38] S. Timoshenko and J. N. Goodier, *Theory Of Elasticity*, 2nd ed. New York: McGraw- Hill, 1951.
- [39] T. L. Anderson, *Fracture Mechanics: Fundamentals and Applications*, 3rd ed. Boca Raton: CRC Press, 2004.